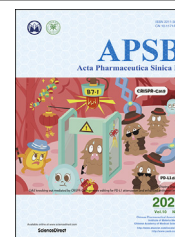




Chinese Pharmaceutical Association  
Institute of Materia Medica, Chinese Academy of Medical Sciences

Acta Pharmaceutica Sinica B

[www.elsevier.com/locate/apsb](http://www.elsevier.com/locate/apsb)  
[www.sciencedirect.com](http://www.sciencedirect.com)



ORIGINAL ARTICLE

# Optimized functional and structural design of dual-target LMRAP, a bifunctional fusion protein with a 25-amino-acid antitumor peptide and GnRH Fc fragment



Meng Li<sup>a,b</sup>, Hanmei Xu<sup>c</sup>, Junzhi Wang<sup>a,b,\*</sup>

<sup>a</sup>Shenyang Pharmaceutical University, Shenyang 110016, China

<sup>b</sup>Key Laboratory of the Ministry of Health for Research on Quality and Standardization of Biotech Products, National Institutes for Food and Drug Control, Beijing 102629, China

<sup>c</sup>State Key Laboratory of Natural Medicines, Ministry of Education, the Engineering Research Center of Synthetic Polypeptide Drug Discovery and Evaluation of Jiangsu Province, Department of Marine Pharmacy, China Pharmaceutical University, Nanjing 211198, China

Received 22 June 2019; received in revised form 19 September 2019; accepted 19 September 2019

## KEY WORDS

Fusion protein;  
GnRH;  
Integrin;  
Angiogenesis;  
Prostate cancer

**Abstract** To develop fusion protein of a GnRH Fc fragment and the integrin targeting AP25 antitumor peptide for GnRH receptor-expressing cancer therapy. The LMRAP fusion protein was constructed. A transwell invasion assay was performed. The gene mRNA and protein levels of GnRHR-I,  $\alpha 5\beta 1$ , and  $\alpha v\beta 3$  in different cancer cell lines were assessed. Cell proliferation was measured using a cell counting kit-8. An antagonist assay was performed on GnRH receptors. Anti-tumor activity was evaluated with a mouse xenograft tumor model. Immunohistochemistry (IHC) was applied to detect CD31 and CD34 expressions. Pharmacokinetic characteristics were determined with an indirect competition ELISA. The developed bifunctional fusion protein LMRAP not only inhibited HUVEC invasion, but also inhibited proliferation of GnRHR-I,  $\alpha 5\beta 1$ , and  $\alpha v\beta 3$  high expression cancer cells. The  $IC_{50}$  for LMRAP in the GnRH receptor was  $6.235 \times 10^{-4}$  mol/L. LMRAP significantly inhibited human prostate cancer cell line 22RV1 proliferation *in vivo* and *in vitro*. LMRAP significantly inhibited CD31 and CD34 expressions. The elimination half-life of the fusion protein LMRAP was 33 h in rats. The fusion protein made of a

\*Corresponding author.

E-mail address: [wangjz\\_nifdc2014@163.com](mailto:wangjz_nifdc2014@163.com) (Junzhi Wang).

Peer review under responsibility of Institute of Materia Medica, Chinese Academy of Medical Sciences and Chinese Pharmaceutical Association.

<https://doi.org/10.1016/j.apsb.2019.10.010>

2211-3835 © 2020 Chinese Pharmaceutical Association and Institute of Materia Medica, Chinese Academy of Medical Sciences. Production and hosting by Elsevier B.V. This is an open access article under the CC BY-NC-ND license (<http://creativecommons.org/licenses/by-nc-nd/4.0/>).

GnRH Fc fragment and the integrin targeting AP25 peptide retained the bifunctional biological activity of GnRHR blocking, angiogenesis inhibition, prolonged half-life and good tolerance.

© 2020 Chinese Pharmaceutical Association and Institute of Materia Medica, Chinese Academy of Medical Sciences. Production and hosting by Elsevier B.V. This is an open access article under the CC BY-NC-ND license (<http://creativecommons.org/licenses/by-nc-nd/4.0/>).

## 1. Introduction

Hypothalamic decapeptide gonadotropin releasing hormone (GnRH), sometimes called luteinizing hormone-releasing hormone (LHRH), has an important role in mammalian reproduction regulation<sup>1</sup>. It has been shown that 86% of human prostate adenocarcinomas have high-affinity binding sites for GnRH. The GnRH receptor (GnRHR) has been detected at lower levels in the normal prostate compared to prostate cancer specimens. Some normal human prostate cell lines have no GnRH signaling<sup>2</sup>. Higher Gleason score tumors have fewer receptor numbers, but have higher affinity receptors<sup>3</sup>. In addition to prostate cancer, breast, endometrial, ovarian, pancreatic and hepatoma cancers, as well as endometrial cells in endometriosis, have cells that express GnRHR<sup>4</sup>. About 50% of breast cancers and 80% of endometrial cancers express both GnRH and GnRHR within the autocrine system<sup>5</sup>.

The neutralizing effect of LHRH/GnRH with hormone-specific antibodies has been established in a wide range of species. Some studies have used passive immunization based on infusion of anti-LHRH antibodies<sup>6</sup>. GnRH vaccines have also been promising for managing hormone-dependent breast and prostate cancers<sup>7–9</sup>. However, the use of these vaccines clinically requires powerful adjuvant therapy to enhance antibody responses that could effectively block hormone–receptor binding<sup>10</sup>.

AP25 is a polypeptide that was designed in our laboratory by modifying an endostatin-derived peptide fragment, which was a 25-amino-acid arginine-glycine-aspartic acid (RGD)-modified polypeptide targeting  $\alpha v\beta 3$  and  $\alpha 5\beta 1$  integrins expressed in endothelial and tumor cells. Previous *in vivo* and *in vitro* experiments have indicated that this integrin antagonist peptide has an extraordinary antitumor effect on different types of cancer<sup>11</sup>.

In this study, we developed a new strategy for GnRH receptor-expressing cancers by fusion of a GnRH Fc (fragment crystallizable) fragment and the AP25 antitumor peptide. The design idea was to maintain the antitumor epitope and activity of both AP25 and the GnRH Fc fragment. The direct fusion of functional domains may lead to misfolding of a product<sup>12</sup>, a low yield<sup>13</sup>, or impaired bioactivity or half-life<sup>14</sup>. The choice of a peptide linker that has the ability to maintain the domain function in the design of a bifunctional fusion protein is essential for maintaining bioactive molecules with an enhanced effect. By choosing a suitable peptide linker (flexible linker) and optimizing the structure of the fusion protein, we hypothesized that the bifunctional fusion protein may possess functions derived from each of their component moieties and this may achieve enhanced therapeutic effects.

## 2. Materials and methods

### 2.1. Animals

Male BALB/c nude mice that were 6–8 weeks old, male and female BALB/c mice, and Sprague–Dawley (SD) rats were

purchased from the Nanjing Model Animal Research Center (Nanjing, China). All animals were given water and sterilized food. The Animal Care and Use Committee of the Nanjing Han and Zaenker Cancer Institute approved the study and it was strictly performed according to the Guide for the Care and Use of Laboratory Animals.

### 2.2. Cell culture, antibodies and reagents

Peptide AP25 was synthesized by GL Biochem (purity > 95%). CD31 and CD34 antibodies were purchased from EnoGene (New York, NY, USA). Human prostate cancer 22RV1, DU145, PC-3, LNCap, human cervical cancer HeLa, SiHa, human ovarian cancer A2780, SW626, OVCAR-3, and SKOV3 cells were purchased from the American Type Culture Collection (ATCC, Manassas, VA, USA). All cells were routinely cultured in Roswell Park Memorial Institute-1640 medium (RPMI-1640, Gibco, Grand Island, NY, USA) with 10% fetal bovine serum (FBS, Gibco), 100  $\mu\text{g}/\text{mL}$  streptomycin (Gibco), and 100 Units/mL penicillin (Gibco) and then maintained at 37 °C in a humidified incubator with 5% CO<sub>2</sub>.

### 2.3. Optimized structures of fusion proteins in the LMRAP series including linkers

The sequence of AP25 was: ACDCRGDCFCGGGGIVRRADRA AVP.

The sequence of LMRAP, GnRH-linker-hIgG4 Fc-linker-AP25 was: PHWSYGLRPGGGGGGGGGGGGGGGGGGGSESKYGPPCPSCP APEFLGGPSVFLFPPKPKDTLMISRTPEVTCVVVDVSDQEDPE VQFNWYVDGVEVHNAKTKPREEQFNSTYRVVSVLTVLHQD WLNQKEYKCKVSNKGLPSSIEKTIKAKGQPREPQVYTLT PPSQEEMTKNQVSLTCLVKGFYPSDIAVEWESNGQPENNYK TTPPVLDSDGSFFLYSRLTVDKSRWQEGNVFSCSVMEAL HNHYTQKSLSLSGGGGGGGGGGGGGGGGGGGIVRRADRAAVPGG GGACDCRGDCFC.

The sequence of LMRAP-A, AP25-linker-hIgG4 Fc-linker-GnRH was: ACDCRGDCFCGGGGIVRRADRAAVPGGGGGGGGGGGGGGGGGGGSESKYGPPCPSCAPEFLGGPSVFLFPPKPKDTL MISRTPEVTCVVVDVSDQEDPEVQFNWYVDGVEVHNAKTK PREEQFNSTYRVVSVLTVLHQD WLNQKEYKCKVSNKGLPSSIEKTIKAKGQPREPQVYTLT PPSQEEMTKNQVSLTCLVKGFYPSDIAVEWESNGQPENNYK TTPPVLDSDGSFFLYSRLTVDKSRWQEGNVFSCSVMEALHNH YTQKSLSLSGGGGGGGGGGGGGGGGGGGIVRRADRAAVPGG GGSGGGGGSPHWSYGLRPG.

The sequence of LMRAP-B, AP25-linker-GnRH-linker-hIgG4 Fc was: ACDCRGDCFCGGGGIVRRADRAAVPGGGGGGGGGGGGGGGGGGGSPHWSYGLRPGGGGGGGGGGGGGGGGGGGSESKYGPPCP SCPAPEFLGGPSVFLFPPKPKDTLMISRTPEVTCVVVDVSDQEDPEVQFNWYVDGVEVHNAKTKPREEQFNSTYRVVSVLTV LHQD WLNQKEYKCKVSNKGLPSSIEKTIKAKGQPREPQV YTLPPSQEEMTKNQVSLTCLVKGFYPSDIAVEWESNGQPEN

NYKTTTPVLDSGDSFFLYSRLTVDKSRWQEGNVFSCSVMH  
EALHNHYTQKSLSL.

Fig. 1A shows the domain arrangements of LMRAP, LMRAP-A, and LMRAP-B.

#### 2.4. Construction of vectors

The target genes of the three fusion proteins were cloned into EcoRI loci of the plasmid vector pEE12.4 by homologous recombination. The host bacteria were Trans1-T1 cells (Transgen Biotech, Beijing, China). TAA/TGA was set as the termination codon. After transformation, a transformed single colony was selected and inoculated into 2 mL Luria-Bertani (LB) medium containing ampicillin resistance. After 6–7 h of incubation at 37 °C and shaking at 220 rpm (thermostatic oscillator, Taicang, China), the sequence of the correct bacterial solution was transferred to 300 mL LB medium containing ampicillin resistance with a 0.5% inoculation amount. After 16 h of shaking the culture at 37 °C and 220 rpm (thermostatic oscillator), stable transfection plasmids were prepared with a Nucleo Bond Xtra Midi Plus EF (MN) kit (Macherey-Nagel, Düren, Germany).

#### 2.5. Stable transfection screening

The recombinant plasmid was transfected into Chinese hamster ovary (CHO)-K1 cells with a neon electrophoresis apparatus under the conditions of 1400 V, 20 ms and 2 pulses. Subsequent to transfection, the cells were incubated in 5 mL 4 mmol/L Gln-containing Dynamis (Gibco) medium that was preheated to 37 °C for two days. They were then inoculated in 96-well plates at 5000 cells/well for three weeks. The cells were screened with 50 µmol/L L-methionine sulfoximine (MSX, Sigma-Aldrich, St. Louis, MO, USA) at 37 °C and cultured in a 7% CO<sub>2</sub> incubator for 3 weeks. The highly expressed clones that were grown in 96-well plates were subcultured from 96-well plates to 24-well stationary plates, and then were cultured again in 24-well plates. The volume of each hole was 2 mL, and the culture medium was Dynamis + 25 µmol/L MSX. The culture conditions were 37 °C, 5% CO<sub>2</sub>, and 220 rpm (thermostatic oscillator). Cells in the 24 deep-hole plates were diluted for 2–4 passages at a density of 0.3–0.5 × 10<sup>6</sup>/mL until the clones adapted to the suspension culture. The clones with the highest expression levels were selected for production and preparation of protein samples.

#### 2.6. Production and affinity chromatography purification of the fusion proteins LMRAP, LMRAP-A and LMRAP-B

Cells were inoculated in 1 L Dynamis medium at a density of 0.5 × 10<sup>6</sup>/mL. The cells were fed batch culture for 14 days on a shaking bed of 37 °C, 5% CO<sub>2</sub> and 130 rpm (thermostatic oscillator). On the third day, the temperature was dropped to 34 °C, and on the third, fifth, seventh and tenth days, the cells were fed with 2 × CD Efficient Feed C<sup>+</sup> (Gibco) at 5%, 5%, 8% and 8% of the culture volume, respectively. On the seventh and tenth days, sugar was added at 3 g/L after nova detection and then the cells were harvested for 14 days. After centrifugation for 15 min, the supernatant was collected and filtered through a 0.45 µm membrane to collect the filtrate. The target protein was an Fc fusion protein, which could be captured by specific adsorption of an Fc fragment with the affinity filler Prosep Ultra Plus (Millipore, Burlington, Massachusetts, USA). First, the column was balanced with a three-fold column volume equilibrium solution, phosphate buffered

saline (PBS, Sigma-Aldrich) at pH 7.0. After balancing, the retention time of the sample was controlled between 1 and 2 min according to the actual pressure of the column. After sampling, the column was washed with a five-fold column volume equilibrium solution. The protein sample was eluted with 50 mmol/L NaAc-HAc (Sigma-Aldrich), pH 3.6 buffer solution, and the retention time was controlled at 3 min. The ultraviolet (UV) value was observed for collection. Protein samples were quantified by 3 mol/L Tris (Sigma-Aldrich) with pH ranging from 6.0 to 7.0.

#### 2.7. Ultrafiltration concentration

Ultrafiltration membranes with a pore size of 30 kD and membrane area of 0.14 m<sup>2</sup> were selected. The membrane was coated with 50 mmol/L phosphate buffer (PB, Sigma-Aldrich) and the displacement solution was pH 6.6. The pH in tank was the same as that in the displacement solution. The filter end was closed and the sample was slowly poured into the tank. The sample was recycled. After the concentration of the sample was stable, the filter end was opened, the volume concentration was controlled to the theoretical volume, and the filter end was closed for internal circulation. When the concentration was stable, the inlet and outlet were opened and the speed of the inlet and outlet was adjusted until a stable volume remained unchanged. After 10 volume changes, closing the inlet and outlet, and concentrating the sample to a certain volume, the outlet was closed. The internal circulation lasted for 30 min. After the internal circulation, the reflux end was opened to collect samples. A certain volume of displacement solution was poured in, the ultrafiltration equipment was washed, and the sample was collected. The final sample system was 50 mmol/L PB and 6% sucrose (Sigma-Aldrich) and the pH was 6.6. The protein was then quantified.

#### 2.8. Confirmation of proteins sequences with liquid chromatography-mass spectrometer (LC-MS)

A filter-aided sample preparation (FASP)<sup>15</sup> method was employed for enzymatic hydrolysis to obtain three final products. A total of 200 µg of proteins were combined with 30 µL SDT buffer [4% sodium dodecyl sulfonate (SDS, Sigma-Aldrich), 100 mmol/L dithiothreitol (DTT, Sigma-Aldrich), 150 mmol/L Tris-HCl (Sigma-Aldrich) pH 8.0]. Using repeated ultrafiltration (Microcon units, 10 kD), DTT, the detergent, and other low-molecular-weight components were removed with UA buffer (8 mol/L Urea, 150 mmol/L Tris-HCl pH 8.0). Next, 100 µL of 100 mmol/L iodoacetamide (IAM, Sigma-Aldrich) in UA buffer were added to block the reduced cysteine residues and the samples were then incubated in darkness for 30 min. The filters were washed three times with 100 µL UA buffer and then twice with 100 µL 25 mmol/L NH<sub>4</sub>HCO<sub>3</sub> (Sigma-Aldrich) buffer. Finally, 4 µg of trypsin (Promega, Madison, WI, USA) in 40 µL 25 mmol/L NH<sub>4</sub>HCO<sub>3</sub> buffer were used to digest the protein suspensions overnight at 37 °C. The resulting peptides were then obtained as a filtrate. The peptides from each sample were desalted on C18 Cartridges [Empore™ SPE Cartridges C18 (standard density), volume 3 mL, bed I.D. 7 mm, Sigma-Aldrich], concentrated with vacuum centrifugation and then reconstituted in 40 µL of 0.1% (v/v) formic acid. The peptide content was estimated using UV light spectral density at 280 nm with an extinction coefficient of 1.1 of a 0.1% (w/v) solution that was calculated based on the frequency of tyrosine and tryptophan in vertebrate proteins.

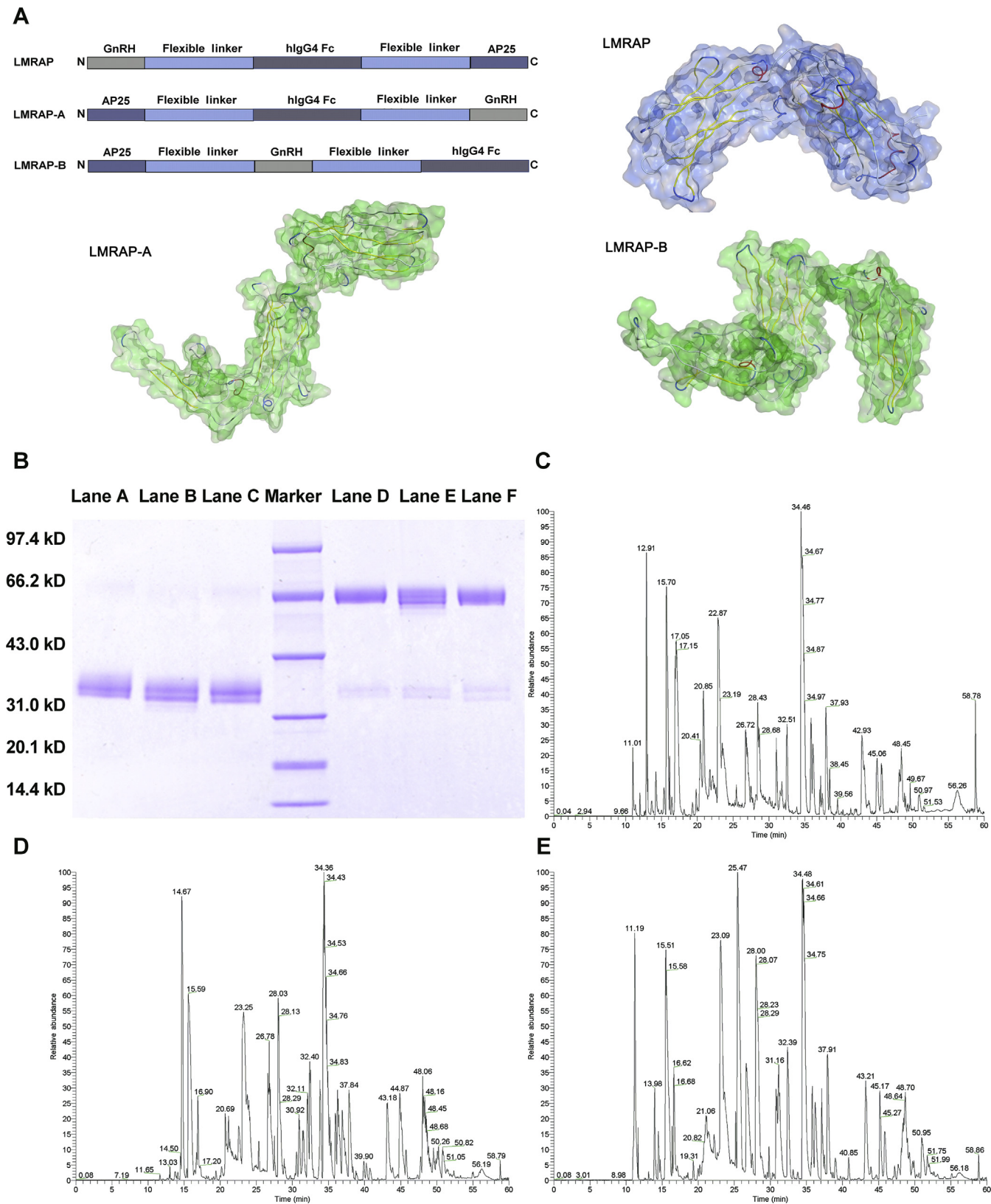


**Figure 1** Schematic of the domain arrangements and structural identifications of LMRAP, LMRAP-A, and LMRAP-B. (A) Schematic of LMRAP, LMRAP-A, and LMRAP-B domain arrangements. (B) SDS-PAGE analyses of the final products after being purified with affinity filler Prosep Ultra Plus. Marker: molecular weight marker; Lanes A–C: LMRAP-A (reduced), LMRAP-B (reduced), LMRAP (reduced), respectively; Lanes D–F: LMRAP-A (non-reduced), LMRAP-B (non-reduced), LMRAP (non-reduced), respectively. Confirmation of proteins sequences with LC–MS of LMRAP (C), LMRAP-A (D), LMRAP-B (E).

A Q Exactive mass spectrometer (Thermo Fisher Scientific, Waltham, MA, USA) that was coupled to an Easy nLC (Proxeon Biosystems, Odense, Denmark) was used for LC–MS/MS analysis for 60 min, which was set in the project proposal<sup>16</sup>. The positive ion mode was used in the mass spectrometer. MS data were obtained using a data-dependent top10 method while the most abundant precursor ions were dynamically chosen from the survey scan (300–1800 *m/z*) for high energy collision induced dissociation (HCD) fragmentation. The maximum inject time was set at 10 ms and the automatic gain control (AGC) target was set at 3e6. The duration of dynamic exclusion was 40 s. The survey scans were acquired at *m/z* 200 at a resolution of 70,000. The resolution for the HCD spectra was set at *m/z* 200 at 17,500. The isolation width was set at 2 *m/z* and the normalized collision energy was set at 30 eV. The underfill ratio was defined as 0.1%, which specified the likely minimum percentage of the target value at maximum fill time. The peptide recognition mode was set at Enabled.

MaxQuant software version 1.5.3.17 (Max Planck Institute of Biochemistry in Martinsried, Germany)<sup>17</sup> was used for analysis of the MS data. The target protein sequence database was searched to recognize MS data. The initial search setting was a precursor mass window of 6 ppm. The search employed the enzymatic cleavage rule of Trypsin/P and two missed cleavage sites were maximally allowed. A mass tolerance of 20 ppm was set for fragment ions: missed cleavage = 2, enzyme = trypsin, fixed variable modification was oxidation (M), modification was carbamidomethyl (C), and the decoy database pattern was reverse. A cutoff of 0.01 was used for the global false discovery rate (FDR) for protein and peptide identification<sup>18</sup>.

### 2.9. Antagonist assay on GnRH receptors

Cells (20  $\mu$ L, 10,000/well) were grown with complete medium in 384-well plates to create a CHO-K1/GnRHR/G $\alpha$ 15 stable cell line (Genscript, Nanjing, China). After overnight incubation at 37 °C/5% CO<sub>2</sub>, we added 20  $\mu$ L/well dye and 10  $\mu$ L/well gonadorelin or LMRAP (five-fold dilution, eight concentrations in triplicate) and then incubated the cells for 1 h. The plate was equilibrated at RT for 15 min and the fluorescence was detected using fluorescence image plate reader (FLIPR) Tetra (Molecular Devices, Los Angeles, CA, USA)<sup>19</sup>. A positive antagonist was used as the reference compound for sample concentration determination.

### 2.10. Cell invasion assay

A transwell invasion assay using Boyden chambers (BD Biosciences, Franklin Lakes, NJ, USA) with 8- $\mu$ m pore size membranes coated with Matrigel was used to evaluate the cell invasive ability<sup>20</sup>. Human umbilical vein endothelial cells (HUVECs) were placed into the upper chamber of an insert in serum-free media. Media with 10% FBS was added to the lower chamber. The cells that had invaded through the membrane after several hours of incubation were stained with methanol and 0.1% crystal violet. They were then imaged and counted under a microscope in random fields at 100 $\times$  magnification in each well.

### 2.11. Real-time polymerase chain reaction (PCR)

The mRNA levels of *GnRHR-I*,  $\alpha$ 5 $\beta$ 1, and  $\alpha$ v $\beta$ 3 were measured via real-time PCR. Trizol reagents (Thermo Fisher Scientific) were used for isolating the total RNA from cancer cells according

to the manufacturer's instructions. Cancer cell RNA (1  $\mu$ g) was used in complementary deoxyribonucleic acid (cDNA) synthesis with reverse transcription reagent (Transgen Biotech). cDNA (125 ng) was added to the real-time PCR reaction along with glyceraldehyde 3-phosphate dehydrogenase (*GAPDH*). Primer Premier version 6.0 software (PREMIER Biosoft, Palo Alto, CA, USA) was used to design specific primers and they were then synthesized by Sangon Biotech (Shanghai, China). The primers were as follows: *GnRHR-I* (forward: 5'-GTGTCTTTGCAG-GACCACAG-3'; reverse: 5'-GCCACCATTGTGAAAACTGC-3'),  $\alpha$ 5 (forward: 5'-TGGCCTTCGGTTTACAGTCC-3'; reverse: 5'-GGAGAGCCGAAAGGAAACCA-3'),  $\beta$ 1 (forward: 5'-GCCGCGGAAAAGATG-3'; reverse: 5'-ACAATTTGGCCCTGCTTGTA-3'),  $\alpha$ v (forward: 5'-GACTCCTGCTACCTCTGTGC-3'; reverse: 5'-CGAAGAAATCCACGGCGAAG-3'),  $\beta$ 3 (forward: 5'-CGAGTGCTCTGTGGTCAAT-3'; reverse: 5'-AGAAGTCGT-CACACTGCAG-3'), and the internal control *GAPDH* (forward: 5'-GGTTGCTCTCCTGCGACTTCA-3'; reverse: 5'-TGGTCCAGGGTTTCTTACTCC-3'). A SYBR Real-time PCR Master Mix kit (TOYOBO, Osaka, Japan) was used to amplify messenger ribonucleic acid (mRNA) according to the manufacturer's protocol. The amplification reactions were carried out on an ABI 7500 real-time PCR system (Applied Biosystems, Foster City, CA, USA). The mRNA levels of the target genes for each experimental group were determined from the 2<sup>- $\Delta\Delta$ Ct</sup> value. Each reaction had three replicates per group.

### 2.12. Western blotting analysis

Cellular extracts were prepared by radioimmunoprecipitation assay (RIPA) lysis buffer, and protein concentrations were quantified by Bradford assays (Bio-Rad Laboratories, Hercules, CA, USA). We electrophoresed a total of 40  $\mu$ g protein through 12% sodium dodecyl sulfate-polyacrylamide gel electrophoresis (SDS-PAGE, Bio-Rad Laboratories) gels and electro-transferred it onto polyvinylidene fluoride (PVDF, Bio-Rad Laboratories) membranes. After being blocked with 5% skim milk, membranes were incubated with primary antibodies recognizing mouse anti-human  $\alpha$ v $\beta$ 3 (1:1000; Abcam, Cambridge, UK), rabbit anti-human GnRHR-I, rabbit anti-human  $\alpha$ 5 $\beta$ 1, rabbit anti-human GAPDH (1:1000, EnoGene) and horseradish peroxidase (HRP)-conjugated secondary antibody (1:5000, EnoGene). The immunoreactivity of bands was developed using an electrochemiluminescence (ECL) detection system (Thermo Fisher Scientific). Membranes were scanned and analyzed using an ImageQuant LAS 4000 Chemiluminescence Imaging System (GE Healthcare, Chicago, IL, USA).

### 2.13. Cell viability assay

A cell counting kit (CCK)-8 (EnoGene) was used to assess cell proliferation<sup>21</sup>. Briefly, cells were plated in 96-well plates at a density of 1  $\times$  10<sup>4</sup> cells/well and were allowed to adhere overnight in a humidified atmosphere of 5% CO<sub>2</sub> at 37 °C. Cells were incubated in a series of diluted concentrations of LMRAP. Cytotoxicity was measured by CCK-8 dye coloration after 72 h incubation. A total of 10  $\mu$ L CCK-8 were added to each well. The plates were then incubated at 37 °C for 4 h. The absorbance was measured at 450 nm with a microplate reader (Thermo Fisher Scientific). The IC<sub>50</sub> values were calculated with GraphPad Prism software (San Diego, CA, USA) and four-parameter curve fitting was employed. All experiments were carried out in six duplicates.

#### 2.14. Anti-tumor activity in a mouse xenograft tumor model

LMRAP antitumor activity was assessed in a human prostate carcinoma model by employing the 22RV1 human prostate cancer cell line<sup>22</sup>. The site's Institutional Animal Care and Use Committee approved the experimental protocol. In this experiment, BALB/c nude male mice that were 6–8 weeks old were implanted in the right flank subcutaneously with  $5 \times 10^6$  22RV1 tumor cells. Animals ( $n = 8$  per group,  $n = 16$  in model group) were randomized for a tumor volume of 80–100 mm<sup>3</sup> at 15 days after tumor cell implantation. Animals received a tail vein injection (i.v.) of LMRAP at 12.5, 25, and 50 mg/kg for two weeks, a tail vein injection of AP25 at 20 mg/kg for two weeks, and a muscle injection (i.m.) of gonadorelin at 65 µg/kg for two weeks, AP25 20 mg/kg (i.v.) combined with gonadorelin 65 µg/kg (i.m.) for two weeks or tail vein injection (i.v.) of avastin 20 mg/kg on day 1 and day 8. Tumor size was measured every other day with digital calipers and the formula volume (mm<sup>3</sup>) = length  $\times$  width<sup>2</sup>/2 was used for calculations. The mice were sacrificed at the end of the study by placing them in a CO<sub>2</sub> gas-filled chamber. The excised tumors were then recovered and weighed.

#### 2.15. IHC

Histological sections from formalin fixed paraffin embedded (FFPE) xenograft tumors were used. IHC was applied to detect Cluster of differentiation 31 (CD31) and Cluster of differentiation 34 (CD34) expressions. IHC staining was performed with CD31 antibodies (EnoGene) and CD34 antibodies (EnoGene) at a 1:100 dilution. Immunostaining was carried out using routine methods. Positive signals of CD34 and CD31 were on the cell membrane. We evaluated the intensity of staining with a scale as previously described. The results were assessed using the following categories: staining intensity of null (0), weak (1+), moderate (2+), and strong (3+). Two experienced pathologists judged all IHC staining results independently.

#### 2.16. Determination of LMRAP in SD rat plasma with an indirect competition enzyme-linked immunosorbent assay (ELISA)

The dosage of tail intravenous administration of LMRAP in SD rats (3 females and 3 males) was 12.5 mg/kg. All procedures were approved by the Institutional Ethical Review Committees and conducted under the authority of the Project License. The experimental sampling time points were: SD rats at 5 min before administration and then 0, 5, 10, 30 min, 1, 2, 4, 6, 8, 12, 24, 36, 48, 72, 96, 120, 144, 168, 192, and 216 h after LMRAP administration. The animal weights were recorded. Eye frame blood was collected and the supernatant was centrifuged. Each serum sample of 100–200 µL was stored in an eppendorf (EP) tube at  $-80$  °C. Sampling times were clearly marked.

The standard sample was diluted to a certain concentration gradient with the mixed solution of blank SD rat plasma and PBS. An indirect competitive ELISA was performed and the standard curve was made<sup>23</sup>. The optical density (OD) 450 nm values of standard samples with different concentration gradients were recorded as  $B$ , and the OD<sub>450 nm</sub> values of standard samples without concentration gradients were recorded as  $B_0$ . ELISA Calc software (Customized Applications Inc., Chicago Heights, IL, USA) was used to fit the logit–log linear regression and establish the standard curve. The fitting equation was: let  $P = B/B_0$ ,  $q = 1-p$ ,  $y = \ln(p/q)$ , and  $x = \lg(C)$ , then the equation was  $y = a+b \times X$ .

The results were processed with pharmacokinetic software drug and statistics (DAS) 1.0 (Mathematical Pharmacology Professional Committee of China, Shanghai, China), ELISA Calc (Customized Applications, Inc.), statistic package for social science (SPSS) package (SPSS Inc., Chicago, IL, USA). The OD value ( $n < 3$ ) was calculated with ELISA Calc software and then pharmacokinetic parameters were calculated with DAS 1.0 software.

#### 2.17. Determination of the maximum tolerated dose (MTD)

To determine the MTD, 10 male and 10 female BALB/c mice were randomly assigned to the study. The animals received dose formulations containing LMRAP at various dosages *via* i.v. injection for a single dose in one day. If no obvious toxicity was observed for the single dose, the animals received dose formulations containing LMRAP at various dosages *via* i.v. injection three times a day. The MTD in this study was defined as the highest dose that was tolerated and that did not produce major life-threatening toxicity in the 14-day study duration<sup>24</sup>.

#### 2.18. Statistical analysis

The data are shown as the mean  $\pm$  standard deviation. The significance of the results obtained from both groups was evaluated with a Student's unpaired *t*-test and one way analysis of variance (ANOVA). All statistical analyses were performed with SPSS 18.0 (SPSS, Inc.). A difference was considered statistically significant with a two-tailed *P* value less than 0.05.  $P < 0.01$  was considered to designate a highly significant difference between the values.

### 3. Results

#### 3.1. LMRAP series fusion protein design, expression, production and purification

According to the arrangement of AP25, GnRH, the Fc fragment and the flexible linker sequence, three fusion protein sequences were designed and named LMRAP, LMRAP-A and LMRAP-B. The domain arrangements are presented in Fig. 1A. The target plasmid for each fusion protein was stably transfected into CHO-K1 cells. The clones with the highest expression levels of each fusion protein were selected for production and preparation of protein samples after stable transfection screening. The final products were identified with SDS-PAGE (Fig. 1B). Their primary sequences were confirmed with LC-MS/MS (Fig. 1C–E). The SDS-PAGE results indicated that the reduced molecular weights of three fusion proteins were each 34 kD. According to SDS-PAGE results, the non-reduced molecular weights of three fusion proteins were each 68 kD, indicating the presence of natural dimers. We also confirmed the deglycosylated molecular weight with time-of-flight mass spectrometry (TOF-MS): the reduced molecular weight was 31,007 Da. This result matched the theoretical molecular weight (31,006 Da of monomer) very well. LC-MS/MS peptide mapping analysis indicated that their primary sequences were identical to the theoretical sequences.

#### 3.2. Effect of LMRAP, LMRAP-A and LMRAP-B on invasion of HUVECs

To screen the anti-tumor activities of fusion proteins LMRAP, LMRAP-A and LMRAP-B, their anti-tumor activities were

evaluated by measuring the effect of *in vitro* experiments on the invasion of HUVECs. The results showed that AP25 had significant migration inhibition on HUVECs at 0.8  $\mu\text{mol/L}$ . LMRAP inhibited HUVECs in a dose-dependent manner (Fig. 2A and B).

The inhibition rates of each dose of AP25 in groups of 0.2, 0.4 and 0.8  $\mu\text{mol/L}$  were  $18.9 \pm 8.9\%$ ,  $28.4 \pm 5.2\%$  and  $79.1 \pm 5.3\%$ , respectively. The inhibition rate of Avastin (0.17  $\mu\text{mol/L}$ ) was  $73.9 \pm 3.6\%$ . The inhibition rates of each dose of LMRAP at 0.1, 0.2, 0.4, 0.8 and 1.6  $\mu\text{mol/L}$  were  $45.8 \pm 5.9\%$ ,  $43.8 \pm 18.4\%$ ,  $57.2 \pm 10.2\%$ ,  $76.6 \pm 3.2\%$  and  $84.9 \pm 2.8\%$ , respectively. The inhibition rates of LMRAP-A at each dose of 0.1, 0.2, 0.4, 0.8, and 1.6  $\mu\text{mol/L}$  were  $17.8 \pm 12.8\%$ ,  $3.2 \pm 18.8\%$ ,  $-13.6 \pm 28.7\%$ ,  $44.6 \pm 21.5\%$ , and  $70.7 \pm 9.5\%$ , respectively. The inhibition rates of LMRAP-B in the 0.1, 0.2, 0.4, 0.8, and 1.6  $\mu\text{mol/L}$  groups were  $-27.0 \pm 16.1\%$ ,  $-1.4 \pm 18.6\%$ ,  $-6.6 \pm 7.7\%$ ,  $13.0 \pm 9.3\%$ , and  $28.2 \pm 12.7\%$ , respectively (Fig. 2C).

In this invasion inhibition experiment of AP25 fusion protein samples LMRAP, LMRAP-A, and LMRAP-B, the invasion inhibition activity of samples LMRAP and LMRAP-A at high concentrations was similar to that of AP25. Compared with the blank control group, LMRAP-B did not inhibit the invasion activity of HUVECs at all concentrations.

### 3.3. LMRAP and LMRAP-A inhibited cancer cell proliferation *in vitro*

The mRNA and protein expression levels of GnRHR-I,  $\alpha 5\beta 1$ ,  $\alpha v\beta 3$  were analyzed in human prostate cancer cells (22RV1, DU145, PC-3, and LNCaP), human ovarian cancer (SKOV3,

OVCAR-3, SW626, and A2780) and human cervical-cancer cell lines (SiHa and HeLa). The results shown in Fig. 3 indicate that human prostate cancer 22RV1, human ovarian cancer SKOV3 and human cervical cancer SiHa had high GnRHR-I expression, while human prostate cancer PC-3 and human ovarian cancer A2780 had medium GnRHR-I expression (Fig. 3A and F). Human cervical cancer SiHa, human ovarian cancer SKOV3 and human prostate cancer PC-3 had high  $\alpha 5\beta 1$  expression, while human ovarian cancer A2780, human prostate cancer 22RV1 and DU145 had medium  $\alpha 5\beta 1$  expression (Fig. 3B, C and F). Human ovarian cancer SKOV3 and human cervical-cancer cell lines SiHa and HeLa had high  $\alpha v\beta 3$  expression, while human prostate cancer 22RV1 had medium  $\alpha v\beta 3$  expression (Fig. 3D–F).

Since LMRAP-B showed no obvious inhibitory effect on HUVEC invasion, LMRAP-B was not a good structure for further research. To assess the *in vitro* antiproliferative effect of LMRAP and LMRAP-A, cancer cells with different GnRHR-I,  $\alpha 5\beta 1$ , and  $\alpha v\beta 3$  integrin expression levels were incubated with a series of increasing doses of LMRAP or LMRAP-A. Cell viability was determined with CCK-8. The results shown in Fig. 4 indicate that LMRAP significantly inhibited GnRHR-I,  $\alpha 5\beta 1$ , and  $\alpha v\beta 3$  integrin high-expression cell viability in human prostate cancers 22RV1 and PC-3 (Fig. 4A and D) and human ovarian cancer SKOV3 as well as A2780 cells (Fig. 4B and C) *in vitro* from 6.25 to 12.5  $\mu\text{mol/L}$  ( $P < 0.05$ ), while LMRAP-A inhibited *in vitro* cell viability in 22RV1, PC-3 cells over 50  $\mu\text{mol/L}$ . From 20 to 50  $\mu\text{mol/L}$ , AP25 inhibited cell viability in PC-3 and SiHa cells *in vitro* (Fig. 4D and E). Gonadorelin showed no significant effect on cell proliferation for all tested cells *in vitro*. LMRAP had an

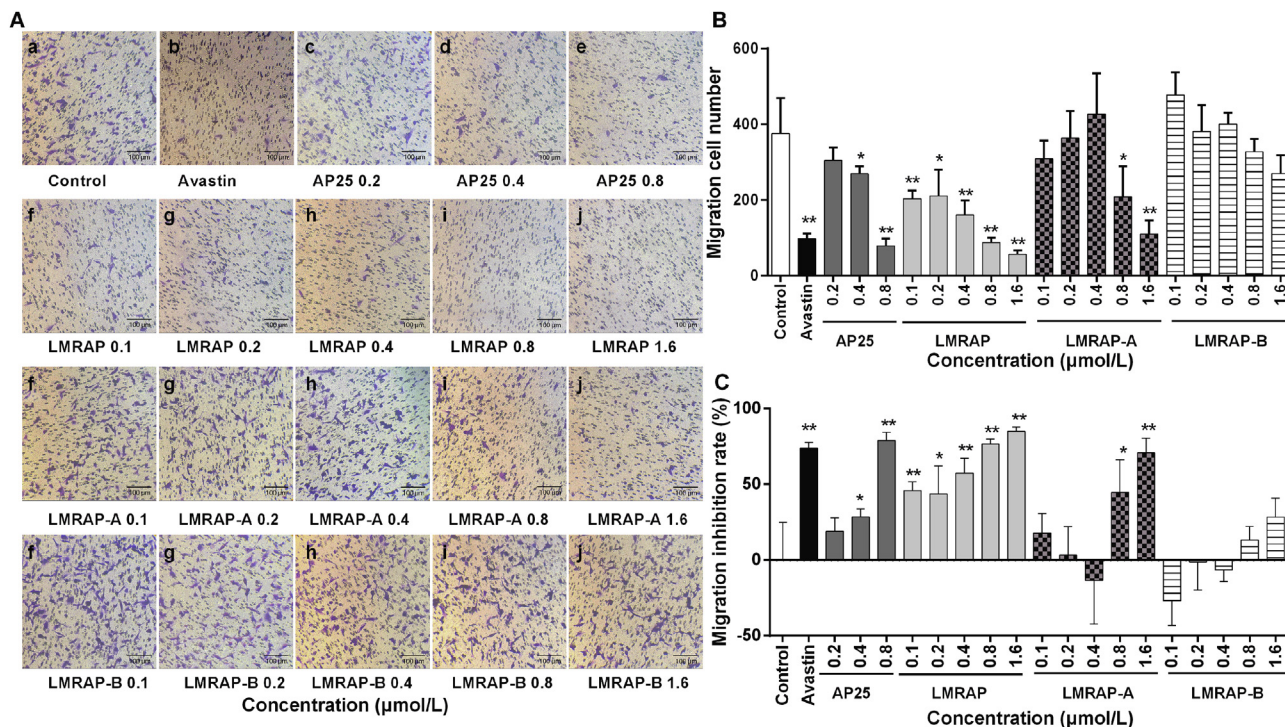


**Figure 2** LMRAP, LMRAP-A, but not LMRAP-B, inhibited the invasion activity of HUVECs. Cell invasive ability was determined with a transwell invasion assay employing Boyden chambers coated with Matrigel. HUVECs in serum-free media were put into the upper chamber of an insert. The cells were then treated with AP25, avastin, LMRAP-A, LMRAP, or LMRAP-B. The cells that had invaded through the membrane were stained with 0.1% crystal violet and methanol. The cells were then imaged and counted in random fields in each well under a microscope at 100 $\times$  magnification. Data are representative of three independent experiments ( $n = 3$ ) (A). The migration cell numbers (B) and the migration inhibition rate (C) are shown based on the number of invasion cells in the experiment in different groups. Data are mean $\pm$ SD; \* $P < 0.05$ , \*\* $P < 0.01$  compared with the control group.

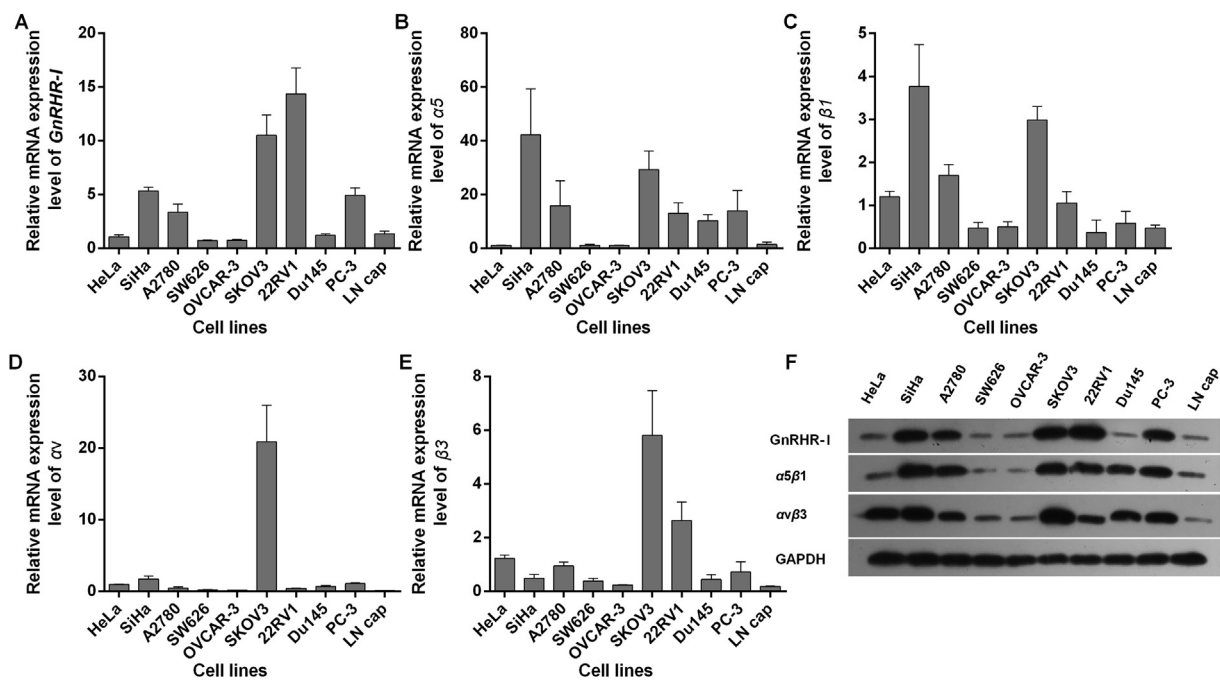


**Figure 3** The mRNA and protein levels of GnRHR-I,  $\alpha 5\beta 1$ , and  $\alpha v\beta 3$  were measured with real-time PCR and Western blot in different cancer cell lines. The SKOV3 human ovarian cancer and 22RV1 human prostate cancer cells had high *GnRHR-I* expression (A). Human cervical cancer SiHa, human prostate cancer PC-3 and human ovarian cancer A2780 had medium *GnRHR-I* expression (A). Human cervical cancer SiHa and human ovarian cancer SKOV3 had high  $\alpha 5\beta 1$  expression. Human ovarian cancer A2780, human prostate cancer 22RV1 and PC-3 had medium  $\alpha 5\beta 1$  expression (B and C). Human ovarian cancer SKOV3 had high  $\alpha v\beta 3$  expression. Human prostate cancer 22RV1 had medium  $\alpha v\beta 3$  expression (D and E). Data are mean $\pm$ SD,  $n=3$ . The protein expression levels of GnRHR-I,  $\alpha 5\beta 1$ , and  $\alpha v\beta 3$  were measured by Western blot in different cancer cell lines (F).

improved cell proliferation inhibitory effect compared with AP25, which indicated that the GnRHR-I-specific binding of LMRAP might promote cytotoxicity of AP25. On the contrary, LMRAP did not show an obvious proliferation inhibition effect on cancer cells with low expression of GnRHR-I,  $\alpha 5\beta 1$ , or  $\alpha v\beta 3$  integrin (Table 1). LMRAP showed the best antiproliferation activity compared with LMRAP-A and AP25.

### 3.4. Functional characterization of LMRAP

Based on computer construction technology, the three parts of AP25, GnRH, and Fc were relatively independent when changing flexible linkers and the combination of spatial structure and

epitope did not affect each other. Antagonist assay results on the GnRH receptors of gonadorelin and LMRAP in a CHO-K1/GnRHR/G $\alpha 15$  stable cell line is shown in Fig. 5. The IC<sub>50</sub>s for gonadorelin (Fig. 5A) and LMRAP (Fig. 5B) were  $1.641 \times 10^{-9}$  and  $6.235 \times 10^{-4}$  mol/L, respectively.

### 3.5. In vivo anti-tumor study of LMRAP

The xenograft tumor model of nude mice was established by s.c. flank injection of human prostate cancer cell line 22RV1. This model was further used to evaluate the therapeutic efficacy of LMRAP *in vivo*. Different doses of LMRAP were injected into the tail vein for 14 consecutive days to evaluate the anti-tumor activity

**Table 1** The IC<sub>50</sub> of LMRAP and LMRAP-A on cells with different expression levels of GnRHR-I and integrin.

Cell line	GnRHR-I	$\alpha 5\beta 1$	$\alpha v\beta 3$	IC <sub>50</sub> ( $\mu$ mol/L)		
				LMRAP	LMRAP-A	AP25
HeLa	±	±	+++	—	—	—
SW626	±	±	+	255.2	290.8	220.9
OVCAR-3	±	±	+	276.2	376.2	352.1
DU145	±	++	++	212.3	—	1354
LNcap	±	+	±	144.8	186.1	229.3
22RV1	+++	++	++	14.42	51.58	818.0
SKOV3	+++	+++	+++	85.38	86.97	990.9
A2780	++	++	++	37.94	122.9	271.2
PC-3	++	+++	++	19.37	60.72	176.6
SiHa	+++	+++	+++	63.74	234.3	137.0

±Very weak expression; +low expression; ++medium expression; +++high expression; —no activity.

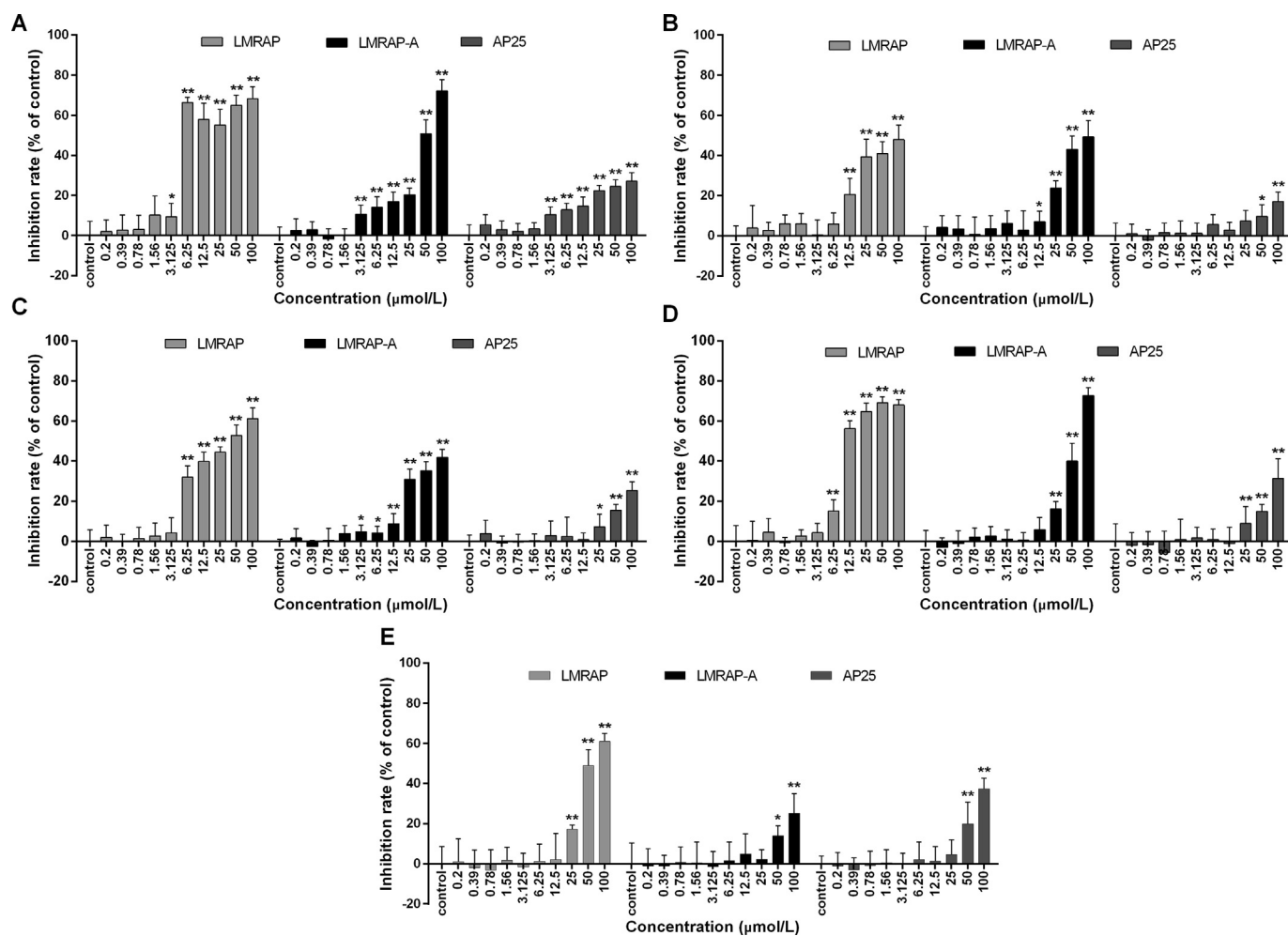


**Figure 4** The *in vitro* antiproliferative effect of LMRAP and LMRAP-A on GnRHR-I expression cells was determined by CCK-8. LMRAP significantly inhibited GnRHR-I positive cell viability in human prostate cancer 22RV1 (A) and PC-3 (D), human ovarian cancer SKOV3 (B), and A2780 (C) cells *in vitro* from 6.25 to 12.5  $\mu\text{mol/L}$ . AP25 itself inhibited cell viability in 22RV1 (A), SKOV3 (B), A2780 (C), PC-3 (D) and SiHa (E) cells *in vitro* from 25 to 50  $\mu\text{mol/L}$ . Data are mean $\pm$ SD,  $n=6$ ; \* $P<0.05$ , \*\* $P<0.01$  vs. Control.

of LMRAP against human prostate cancer. The results showed (Fig. 6A and B) that the relative tumor volume (RTV) of treatment group/RTV of control group (T/C, %) of LMRAP 12.5, 25 and 50 mg/kg for transplanted tumors of 22RV1 nude mice were 56.34%, 47.44%, and 32.16%, respectively, and the inhibition rates were 29.56%, 48.00%, and 61.97%, respectively. The T/C (%) of the control drugs AP25, gonarellin, the AP25/gonarellin combination, and avastin, were 70.83%, 82.19%, 50.52% and 15.23%, respectively, and the inhibition rates were 37.59%, 18.80%, 52.70%, and 82.72%, respectively. There was no significant difference in body weight gain between the treatment group and the model group, which indicated that no general toxicity was caused by the treatments.

### 3.6. IHC staining of CD34 and CD31

Considering the importance of angiogenesis in prostate cancer progression, we further evaluated angiogenesis by IHC analysis of CD34 and CD31 expression in the xenografted 22Rv1 tumors. The results in Fig. 7A and B show that LMRAP significantly inhibited both CD31 and CD34 expression in prostate cancer ( $P < 0.01$ ).

### 3.7. Pharmacokinetic study of LMRAP injected into the tail veins of SD rats

First, the working concentration of coated antigen and monoclonal antibodies was established. The optimal working concentration of coated antibodies and antigens was determined with the square array method. The antigens were diluted to 1:200, 1:400, 1:800, 1:3200, 1:6400, and 1:12,800 times and negative pore, and were

coated transversely into the enzyme plate. After washing, the antibodies were diluted at 1:2 K, 1:4 K, 1:8 K, and 1:16 K and added vertically for ELISA detection.

Finally, the dilution factor of OD<sub>450 nm</sub> equal to 1.0 was chosen as the ideal concentration. According to the test results, the optimal concentration of the antigen was 1:800 and the dilution ratio of the monoclonal antibody was 1:4 K. The dilution ratio of the secondary antibody was 1:2000, which was the optimum concentration. The three batch standard curves of the LMRAP concentration in SD rat plasma ranged from 12,800 to 100 ng/mL. The curve equations were  $y = 6.2824 - 2.0017x$  and  $y = 6.1193 - 1.7859x$  and  $y = 8.1738 - 2.5234x$ . The linear exponents  $R^2$  were 0.9901, 0.9902, and 0.9974, respectively. The intra-batch precision of high (10,000 ng/mL), medium (1000 ng/mL), and low (200 ng/mL) concentration quality control samples was 9.39%, 5.87%, and 7.26%, the inter-batch precision was 10.55%, 7.42%, and 8.14%, and the recovery rates were 111.00%, 97.10%, and 100.64%, respectively.

After tail vein injection of 12.5 mg/kg LMRAP in SD rats, the curve of the blood drug concentration–time is shown in Fig. 8, and the pharmacokinetic parameters are shown in Table 2. The results showed that the pharmacokinetic process of LMRAP in SD rats was a one-compartment model after intravenous administration of 12.5 mg/kg LMRAP. The maximum plasma concentration ( $C_{max}$ ) was  $93.346 \pm 15.722$  µg/mL. The elimination half-life ( $t_{1/2\beta}$ ) was  $33.332 \pm 11.189$  h, area under the concentration–time curve [AUC<sub>(0–216)</sub>] was  $539.94 \pm 155.243$  mg/L·h, clearance (CL) was  $0.038 \pm 0.036$  L/h, and apparent volume of distribution ( $V_d$ ) was  $1.787 \pm 1.527$  L/kg. This method was based on an indirect competitive ELISA for the LMRAP monoclonal antibody, with high specificity and accurate results.

**Table 2** Pharmacokinetic parameters of LMRAP following a single i.v. administration to rat at a dose of 12.5 mg/kg.

Parameter	Unit	Animal						Mean	SD
		1	2	3	4	5	6		
$\alpha, K_e$	$h^{-1}$	0.240	0.000	0.384	0.000	0.000	1.131	0.293	0.402
$t_{1/2\beta}$	h	45.237	29.187	50.979	18.256	27.879	28.452	33.332	11.189
$V_d$	L/kg	1.832	0.419	2.622	0.731	0.426	4.693	1.787	1.527
$T_{max}$	h	0.000	1.000	0.167	0.083	0.500	0.000	0.292	0.359
AUC <sub>(0–216)</sub>	mg/L·h	843.228	612.758	508.935	360.059	470.547	444.113	539.940	155.243
AUC <sub>(0–∞)</sub>	mg/L·h	1931.013	1014.410	1417.535	388.813	521.421	1236.213	1084.901	525.430
CL	L/h/kg	0.028	0.010	0.036	0.027	0.010	0.114	0.038	0.036
$C_{max}$	µg/mL	102.028	94.773	119.001	69.386	80.244	94.646	93.346	15.722

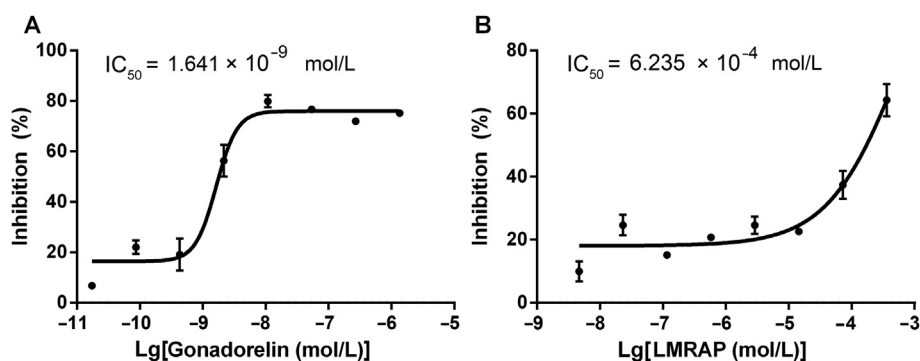


**Figure 5** Functional characterization of LMRAP. The antagonist assay on GnRH receptors of gonadorelin and LMRAP in the CHO-K1/GnRHR/Gα15 stable cell line showed the IC<sub>50</sub> for gonadorelin was  $1.641 \times 10^{-9}$  mol/L (A) and LMRAP was  $6.235 \times 10^{-4}$  mol/L (B). Data are mean ± SD,  $n = 3$ .

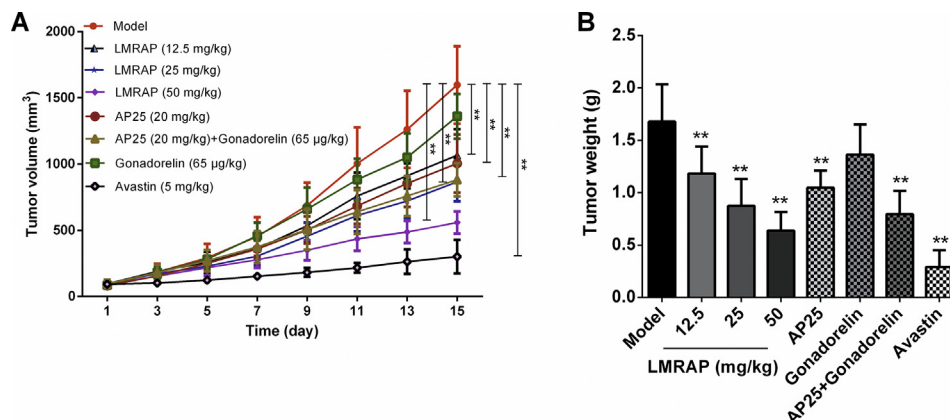


**Figure 6** *In vivo* anti-tumor study of LMRAP. Xenograft 22Rv1 tumors were induced by s.c. flank injection in nude mice. This model was used to assess the therapeutic efficacy of LMRAP *in vivo*. Tumor growth curve (A) and the tumor weight (B) of tumor bearing nude mice showed that the T/C (%) of LMRAP 12.5, 25, and 50 mg/kg for transplanted tumors of 22Rv1 nude mice were 56.34%, 47.44%, and 32.16%, respectively, and the inhibition rates were 29.56%, 48.00%, and 61.97%, respectively.  $^{**}P < 0.01$  compared with the model group (Data are mean $\pm$ SD,  $n = 8$  per group except  $n = 16$  in model group).

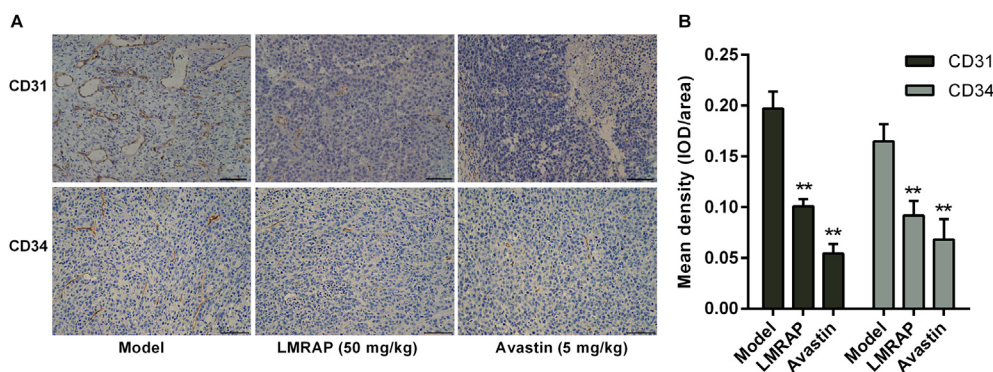


**Figure 7** IHC detection of CD31 and CD34 expressions. Histological sections from FFPE xenograft tumors were used. (A) Positive signal of CD31 and CD34 in the model group, LMRAP (50 mg/kg) and Avastin (5 mg/kg). (B) CD31 and CD34 expression densities were independently assessed. LMRAP significantly inhibited both CD31 and CD34 expressions in prostate cancer. Data are mean $\pm$ SD,  $n = 8$ .  $^{**}P < 0.01$  compared with the model group. The bar = 50  $\mu$ m.

### 3.8. Toxicity of LMRAP in mice

Further determination of the MTD showed that the animals receiving LMRAP at 2560 mg/kg *via* i.v. injection for a single

dose in one day did not show obvious toxicity. The animals received further LMRAP at 2560 mg/kg *via* i.v. injection three times a day. After 14 days' further observation, no animal mortality was observed, nor were there any obvious changes in animal body weight increase or animal behavior. The MTD of LMRAP was 7680 mg/kg *via* i.v. injection, which was 307.2 times of the pharmacodynamic dose (25 mg/kg).

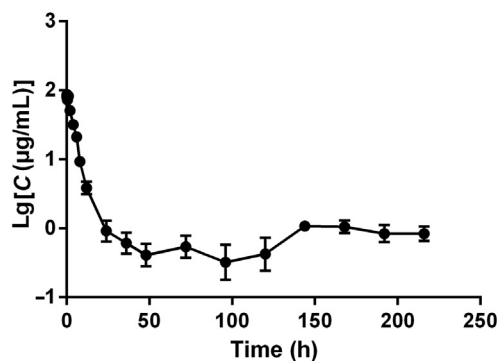


**Figure 8** Plasma concentration–time curve of LMRAP following a single i.v. administration to a rat at a dose of 12.5 mg/kg. Data are mean $\pm$ SD,  $n = 6$ .

## 4. Discussion

Prostate cancer accounts for one-fifth of new cancer diagnoses and it is the third leading cause of cancer death in the United States<sup>25,26</sup>. Androgen deprivation therapy is indicated for use in multiple clinical settings for advanced prostate cancer, which includes chemical castration consisting of GnRH agonists and antagonists<sup>27</sup>. One of the main concerns when using GnRH agonists, such as goserelin or gonadorelin, is a testosterone surge caused by initial stimulation of the pituitary gland, which may lead to a tumor flare, a rapid expansion of the prostate cancer, leading to pain and potential debilitation in patients, specifically with spinal metastases<sup>28</sup>. The GnRH agonists generated considerable side-

effects including hot flashes, impotence, accelerated bone resorption, loss of muscle mass, loss of libido and, in some instances, profound psychologic effects<sup>29</sup>.

An immunological approach to achieve androgen deprivation to treat prostate cancer, such as LHRH vaccinations, had also been tested in men<sup>30</sup>. Passive immunization, that is, infusion of anti-LHRH antibodies that neutralized the action of LHRH/GnRH through the involvement of hormone-specific antibodies, has been demonstrated in many animal species<sup>6</sup>. The GnRH–tetanic toxoid conjugates, due to their large size, can induce anti-haptenic immunosuppression; however, this is difficult to reproduce on an industrial scale<sup>31</sup>. Studies have reported that the administration of either polyvalent or monoclonal anti-GnRH antibodies in males leads to cessation of spermatogenesis, decreased testicular size, and a severe reduction of testosterone levels, as does immunization with GnRH-carrier conjugates<sup>32,33</sup>.

Angiogenesis is an important process that occurs in both physiological and pathological conditions. It has been shown that angiogenesis affects the behavior and biology of various neoplastic and non-neoplastic diseases<sup>34,35</sup>. Angiogenesis plays a crucial role in prostate cancer survival, progression, and metastasis<sup>36–38</sup>. It is a complicated process that depends on the balance between inhibitors and activators of angiogenesis<sup>39</sup>. Vascular endothelial growth factor (VEGF) and several neurosecretory peptides, such as bombesin and gastrin, are known to promote angiogenesis in prostate cancer<sup>40</sup>.

Bifunctional molecules that have been classified as novel therapeutics have been shown to have multifunctional properties<sup>41</sup>. A fusion protein with two or more domains genetically fused together might have improved product stability. This might help with the acquisition of biological activity<sup>42</sup>. AP25 is an anti-angiogenic and anti-tumor peptide with molecular targets, including integrin  $\alpha 5\beta 1$  and  $\alpha v\beta 3$ . AP25 contains the sequence ES-2 and this sequence is included in one of the two active domains of endostatin. It induces the inhibitory effect of endostatin on angiogenesis<sup>43</sup>. GnRH is a hypothalamic decapeptide gonadotropin releasing hormone that binds to the GnRHR that is expressed in cancer cells, such as prostate cancer cells. The Fc fragment is part of the constant region heavy chain 2 ( $C_{H2}$ ) and constant region heavy chain 3 ( $C_{H3}$ ) functional region of IgG, and it can improve the stability and prolong the plasma half-life of a fusion protein. This is due to depressed kidney filtration and degradation prevention when binding to neonatal Fc receptor (FcRn)<sup>44,45</sup>. However, direct fusion of various functional domains may cause misfolding of fusion protein spatial structures, lower potency or inefficient expression<sup>12–14</sup>. To maintain domain function, the choice of a peptide linker in the design for bifunctional fusion is quite significant. Efficacy in the fusion protein domain separation is influenced by linker sequence flexibility. The linker GGGGSGGGGSGGGGS<sup>46</sup>, comprising small size amino acids (Gly, Ser), provides enhanced flexibility and mobility of the connecting functional domains to expose binding areas and avoid the coated Fc fragment, which promotes effective targeting.

LMRAP is an Fc fusion protein produced by the fusion of functional proteins with GnRH Fc fragments and the AP25 peptide using genetic engineering technology. The Fc segment in molecular design originates from IgG4 and has a weak antibody dependent cellular cytotoxicity (ADCC) effect<sup>47</sup>. The fusion protein not only retains the biological activity of the functional proteins, but also prolongs the half-life, reduces glomerular clearance and avoids lysosome hydrolysis in cells. Fusion protein characteristics are influenced in various ways by the flexibility of

the linker sequence<sup>48</sup>. Our study showed that in the sequence of LMRAP, GnRH-linker-hIgG4 Fc-linker-AP25 had the best activity compared with the sequence of LMRAP-A, AP25-linker-hIgG4 Fc-linker-GnRH and the sequence of LMRAP-B, AP25-linker-GnRH-linker-hIgG4 Fc. LMRAP not only significantly inhibited the invasion activity of HUVECs, but also significantly inhibited GnRHR-I positive cell viability in human prostate cancers 22RV1 and PC-3, human ovarian cancer SKOV3, and A2780 cells *in vitro*. The  $IC_{50}$  for LMRAP in GnRH receptors was  $6.235 \times 10^{-4}$  mol/L by antagonist assay. In prostate cancer cells, GnRHR signaling includes activation of phosphoinositide (PI) and Gi turnover<sup>49</sup>. This signaling could further activate protein kinase C (PKC) and result in negative transmodulation of epidermal growth factor receptor (EGFR) due to Thr654 phosphorylation, which is known to downregulate EGFR and inhibit its signaling<sup>50</sup>. In addition, GnRH reduced cyclic adenosine monophosphate (cAMP) levels and EGF binding sites in prostate cancer cells<sup>51</sup>.

LMRAP significantly inhibited human prostate cancer cell line 22RV1 proliferation *in vivo*, which is consistent with the *in vitro* study. This may be caused partly by GnRH receptor blocking. To further investigate whether LMRAP inhibited angiogenesis, microvessel density (MVD) using various endothelial cell markers including CD34 and CD31 were assessed. CD34 is a 110-kDa cell surface glycoprotein and it functions as a cell–cell adhesion factor. It mediates the attachment of stem cells to stromal cells or the bone marrow extracellular matrix. CD31, a 130-kDa glycoprotein, is found on the surface of blood endothelial cells, platelets, lymphocytes, and macrophages. Both CD31 and CD34 can be used to demonstrate the presence of endothelial cells in histological tissue sections to assess tumor angiogenesis<sup>52</sup>. Our study showed that LMRAP significantly inhibited both CD31 and CD34 expression in prostate cancer xenografted tumor tissues, which further confirmed that LMRAP had bifunctional properties. The study of LMRAP pharmacokinetic characteristics in the plasma of SD rats indicated that the elimination half-life of fusion protein LMRAP was prolonged to 33 h compared with the polypeptide AP-25 having an elimination half-life of 55 min. Gonadorelin is not a cytotoxic drug and it cannot directly produce anti-tumor effects in terms of its mechanism of action. In molecular mechanism designs, we introduced the polypeptide AP25, which has anti-tumor effects. Therefore, in this study, the anti-prostate cancer effect of the fusion protein is mainly produced by AP25. Because of the addition of the Gonadorelin domain to the fusion protein, the fusion protein has the additional potential function of regulating the release of the gonadal axis hormone. In addition to the improved pharmacokinetic characteristics, LMRAP was also well tolerated in mice based on the absence of clinical side effects in all animals, minimal body weight and animal activities. The MTD was 307.2 times of the pharmacodynamic dose, which indicated that LMRAP had a good safety performance.

## 5. Conclusions

A new strategy for GnRH expressing cancers was developed by fusing the GnRH Fc fragment and the integrin targeting AP25 antitumor peptide. The fusion protein not only retained the bifunctional biological activity of GnRH receptor blocking and angiogenesis inhibition, but also prolonged the half-life, which provides a reliable basis for the later pre-clinical research. The clinical effect of the fusion protein may have better potential as a therapeutic agent.

## Acknowledgments

The subject of the National Science and Technology Major Projects for Major New Drugs Innovation and Development supported this study (grant No. 2018ZX09736016-007, China).

## Author contributions

Junzhi Wang conceptualized this study. Hanmei Xu and Meng Li designed this study. Meng Li drafted the manuscript. Hanmei Xu conducted the animal experiments and data analysis. Meng Li performed the molecular biology study and pharmaceutical analysis study.

## Conflicts of interest

The authors declare no conflict of interests in this work.

## References

- Stanislaus D, Pinter JH, Janovick JA, Conn PM. Mechanisms mediating multiple physiological responses to gonadotropin-releasing hormone. *Mol Cell Endocrinol* 1998;**144**:1–10.
- Bono AV, Salvatore M, Celato N. Gonadotropin-releasing hormone receptors in prostate tissue. *Anal Quant Cytol Histol* 2002;**24**:221–7.
- Halmos G, Arencibia JM, Schally AV, Davis R, Bostwick DG. High incidence of receptors for luteinizing hormone-releasing hormone (LHRH) and LHRH receptor gene expression in human prostate cancers. *J Urol* 2000;**163**:623–9.
- Imai A, Tamaya T. GnRH receptor and apoptotic signaling. *Vitam Horm* 2000;**59**:1–33.
- Emons G, Grundker C, Gunthert AR, Westphalen S, Kavanagh J, Verschraegen C. GnRH antagonists in the treatment of gynecological and breast cancers. *Endocr Relat Cancer* 2003;**10**:291–9.
- Silversides DW, Murphy BD, Misra V, Mapletoft RJ. Monoclonal antibodies against LHRH: development and immunoactivity *in vivo* and *in vitro*. *J Reprod Immunol* 1985;**7**:171–84.
- Xu J, Zhu Z, Wu J, Liu W, Shen X, Zhang Y, et al. Immunization with a recombinant GnRH vaccine conjugated to heat shock protein 65 inhibits tumor growth in orthotopic prostate cancer mouse model. *Cancer Lett* 2008;**259**:240–50.
- Fromme B, Eftekhari P, Van Regenmortel M, Hoebeke J, Katz A, Millar R. A novel retro-inverso gonadotropin-releasing hormone (GnRH) immunogen elicits antibodies that neutralize the activity of native GnRH. *Endocrinology* 2003;**144**:3262–9.
- Hsu CT, Ting CY, Ting CJ, Chen TY, Lin CP, Whang-Peng J, et al. Vaccination against gonadotropin-releasing hormone (GnRH) using toxin receptor-binding domain-conjugated GnRH repeats. *Cancer Res* 2000;**60**:3701–5.
- Ferro VA, Stimson WH. Investigation into suitable carrier molecules for use in an anti-gonadotrophin releasing hormone vaccine. *Vaccine* 1998;**16**:1095–102.
- Yin R, Zheng H, Xi T, Xu HM. Effect of RGD-4C position is more important than disulfide bonds on antiangiogenic activity of RGD-4C modified endostatin derived synthetic polypeptide. *Bioconjug Chem* 2010;**21**:1142–7.
- Zhao HL, Yao XQ, Xue C, Wang Y, Xiong XH, Liu ZM. Increasing the homogeneity, stability and activity of human serum albumin and interferon- $\alpha$ 2b fusion protein by linker engineering. *Protein Expr Purif* 2008;**61**:73–7.
- Amet N, Lee HF, Shen WC. Insertion of the designed helical linker led to increased expression of TF-based fusion proteins. *Pharm Res* 2009;**26**:523–8.
- Bai Y, Ann DK, Shen WC. Recombinant granulocyte colony-stimulating factor-transferrin fusion protein as an oral myelopoietic agent. *Proc Natl Acad Sci U S A* 2005;**102**:7292–6.
- Wisniewski JR, Zougman A, Nagaraj N, Mann M. Universal sample preparation method for proteome analysis. *Nat Methods* 2009;**6**:359–62.
- Leutert M, Menzel S, Braren R, Rissiek B, Hopp AK, Nowak K, et al. Proteomic characterization of the heart and skeletal muscle reveals widespread arginine ADP-ribosylation by the ARTC1 ectoenzyme. *Cell Rep* 2018;**24**:1916–29. e5.
- Cox J, Mann M. MaxQuant enables high peptide identification rates, individualized p.p.b.-range mass accuracies and proteome-wide protein quantification. *Nat Biotechnol* 2008;**26**:1367–72.
- Mann K, Edsinger E. The Lottia gigantea shell matrix proteome: re-analysis including MaxQuant iBAQ quantitation and phosphoproteome analysis. *Proteome Sci* 2014;**12**:28.
- Ciechanowska M, Kowalczyk M, Lapot M, Malewski T, Antkowiak B, Brytan M, et al. Effect of corticotropin releasing hormone and corticotropin releasing hormone nist on biosynthesis of gonadotropin releasing hormone and gonadotropin releasing hormone receptor in the hypothalamic-pituitary unit of follicular-phase ewes and contribution of kisspeptin. *J Physiol Pharmacol* 2018;**69**:451–61.
- Liu K, Tian T, Zheng Y, Zhou L, Dai C, Wang M, et al. Scutellarin inhibits proliferation and invasion of hepatocellular carcinoma cells via down-regulation of JAK2/STAT3 pathway. *J Cell Mol Med* 2019;**23**:3040–4.
- Ramos-Alvarez I, Jensen RT. P21-activated kinase 4 in pancreatic acinar cells is activated by numerous gastrointestinal hormones/neurotransmitters and growth factors by novel signaling, and its activation stimulates secretory/growth cascades. *Am J Physiol Gastrointest Liver Physiol* 2018;**315**:G302–17.
- Fidanzu-Dugas C, Liagre B, Chemin G, Perraud A, Carrion C, Couquet CY, et al. Analysis of the *in vitro* and *in vivo* effects of photodynamic therapy on prostate cancer by using new photosensitizers, protoporphyrin IX-polyamine derivatives. *Biochim Biophys Acta Gen Subj* 2017;**1861**:1676–90.
- Bjornsdottir I, Sternebring O, Kappers WA, Selvig H, Korno HT, Kristensen JB, et al. Pharmacokinetics, tissue distribution and excretion of 40 kDa PEG and PEGylated rFVIII (N8-GP) in rats. *Eur J Pharm Sci* 2016;**87**:58–68.
- Robinson S, Delongas JL, Donald E, Dreher D, Festag M, Kervyn S, et al. A European pharmaceutical company initiative challenging the regulatory requirement for acute toxicity studies in pharmaceutical drug development. *Regul Toxicol Pharmacol* 2008;**50**:345–52.
- Siegel RL, Miller KD, Fedewa SA, Ahnen DJ, Meester RGS, Barzi A, et al. Colorectal cancer statistics, 2017. *CA Cancer J Clin* 2017;**67**:177–93.
- Zhou M, Li L, Li L, Lin X, Wang F, Li Q, et al. Overcoming chemotherapy resistance via simultaneous drug-efflux circumvention and mitochondrial targeting. *Acta Pharm Sin B* 2019;**9**:615–25.
- Dlugi AM, Miller JD, Knittle J. Lupron depot (leuprolide acetate for depot suspension) in the treatment of endometriosis: a randomized, placebo-controlled, double-blind study. Lupron Study Group. *Fertil Steril* 1990;**54**:419–27.
- Lebret T, Culine S, Davin JL, Hennequin C, Mignard JP, Moreau JL, et al. Quality of life of 1276 elderly patients with prostate cancer, starting treatment with a gonadotropin-releasing hormone agonist: results of a French observational study. *Aging Male* 2014;**17**:87–93.
- Chang JI, Bucci J. Unusual side effect from a luteinizing hormone-releasing hormone agonist, leuprorelin, in the treatment of prostate cancer: a case report. *J Med Case Rep* 2016;**10**:323.
- Finstad CL, Wang CY, Kowalski J, Zhang M, Li ML, Li XM, et al. Synthetic luteinizing hormone releasing hormone (LHRH) vaccine for effective androgen deprivation and its application to prostate cancer immunotherapy. *Vaccine* 2004;**22**:1300–13.
- Etlinger HM, Gillessen D, Lahm HW, Matile H, Schonfeld HJ, Trzeciak A. Use of prior vaccinations for the development of new vaccines. *Science* 1990;**249**:423–5.

32. Schutze MP, Leclerc C, Jolivet M, Audibert F, Chedid L. Carrier-induced epitopic suppression, a major issue for future synthetic vaccines. *J Immunol* 1985;**135**:2319–22.
33. Sad S, Chauhan VS, Arunan K, Raghupathy R. Synthetic gonadotrophin-releasing hormone (GnRH) vaccines incorporating GnRH and synthetic T-helper epitopes. *Vaccine* 1993;**11**:1145–50.
34. Zuazo-Gaztelu I, Casanovas O. Unraveling the role of angiogenesis in cancer ecosystems. *Front Oncol* 2018;**8**:248.
35. Cui C, Merritt R, Fu L, Pan Z. Targeting calcium signaling in cancer therapy. *Acta Pharm Sin B* 2017;**7**:3–17.
36. Li Y, Cozzi PJ. Angiogenesis as a strategic target for prostate cancer therapy. *Med Res Rev* 2010;**30**:23–66.
37. Villaume K, Blanc M, Gouysse G, Walter T, Couderc C, Nejjarri M, et al. VEGF secretion by neuroendocrine tumor cells is inhibited by octreotide and by inhibitors of the PI3K/AKT/mTOR pathway. *Neuroendocrinology* 2010;**91**:268–78.
38. Yazdani S, Kasajima A, Tamaki K, Nakamura Y, Fujishima F, Ohtsuka H, et al. Angiogenesis and vascular maturation in neuroendocrine tumors. *Hum Pathol* 2014;**45**:866–74.
39. Carmeliet P, Jain RK. Angiogenesis in cancer and other diseases. *Nature* 2000;**407**:249–57.
40. Heinrich E, Trojan L, Friedrich D, Voss M, Weiss C, Michel MS, et al. Neuroendocrine tumor cells in prostate cancer: evaluation of the neurosecretory products serotonin, bombesin, and gastrin—impact on angiogenesis and clinical follow-up. *Prostate* 2011;**71**:1752–8.
41. Kim BJ, Zhou J, Martin B, Carlson OD, Maudsley S, Greig NH, et al. Transferrin fusion technology: a novel approach to prolonging biological half-life of insulinotropic peptides. *J Pharmacol Exp Ther* 2010;**334**:682–92.
42. Arnau J, Lauritzen C, Petersen GE, Pedersen J. Current strategies for the use of affinity tags and tag removal for the purification of recombinant proteins. *Protein Expr Purif* 2006;**48**:1–13.
43. Hu J, Cheng T, Zhang L, Sun B, Deng L, Xu H. Anti-tumor peptide AP25 decreases cyclin D1 expression and inhibits MGC-803 proliferation via phospho-extracellular signal-regulated kinase-, Src-, c-Jun N-terminal kinase- and phosphoinositide 3-kinase-associated pathways. *Mol Med Rep* 2015;**12**:4396–402.
44. Kim NA, An IB, Lim HS, Yang SI, Jeong SH. Biophysical evaluation of hybrid Fc fusion protein of hGH to achieve basal buffer system. *Int J Pharm* 2016;**513**:421–30.
45. Roopenian DC, Akilesh S. FcRn: the neonatal Fc receptor comes of age. *Nat Rev Immunol* 2007;**7**:715–25.
46. Bai Y, Shen WC. Improving the oral efficacy of recombinant granulocyte colony-stimulating factor and transferrin fusion protein by spacer optimization. *Pharm Res* 2006;**23**:2116–21.
47. Kellner C, Derer S, Klausz K, Roskopf S, Wirt T, Rosner T, et al. Fc Glyco- and Fc protein-engineering: design of antibody variants with improved ADCC and CDC activity. *Methods Mol Biol* 2018;**1827**:381–97.
48. Huang Z, Zhang C, Chen S, Ye F, Xing XH. Active inclusion bodies of acid phosphatase PhoC: aggregation induced by GFP fusion and activities modulated by linker flexibility. *Microb Cell Fact* 2013;**12**:25.
49. Pemberton JG, Stafford JL, Chang JP. Ligand-selective signal transduction by two endogenous GnRH isoforms involves biased activation of the class I PI3K catalytic subunits p110 $\beta$ , p110 $\gamma$ , and p110 $\delta$  in pituitary gonadotropes and somatotropes. *Endocrinology* 2015;**156**:218–30.
50. Aifa S, Frikha F, Miled N, Johansen K, Lundstrom I, Svensson SP. Phosphorylation of Thr654 but not Thr669 within the juxtamembrane domain of the EGF receptor inhibits calmodulin binding. *Biochem Biophys Res Commun* 2006;**347**:381–7.
51. Moretti RM, Monagnani Marelli M, van Groeninghen JC, Motta M, Limonta P. Inhibitory activity of luteinizing hormone-releasing hormone on tumor growth and progression. *Endocr Relat Cancer* 2003;**10**:161–7.
52. Sidney LE, Branch MJ, Dunphy SE, Dua HS, Hopkinson A. Concise review: evidence for CD34 as a common marker for diverse progenitors. *Stem Cells* 2014;**32**:1380–9.